Title

- **The Role of PKR on Modulating Neuroinflammation and Cognitive Dysfunctions in a Peripheral Inflammation Model**

Authors

Wai-Yin Cheng,[1,2,3]*, Xin-Zin Lee,[1] Michael Siu-Lun Lai,[1] Yuen-Shan Ho,[4] Raymond Chuen-Chung Chang [1,5]*

Affiliations

[1]Laboratory of Neurodegenerative Diseases, School of Biomedical Sciences, LKS Faculty of Medicine, The University of Hong Kong, Hong Kong SAR, China

[2]Research Institute for Future Food, The Hong Kong Polytechnic University, Hung Hom, Kowloon, Hong Kong SAR, China

[3]Department of Food Science and Nutrition, The Hong Kong Polytechnic University, Hung Hom, Kowloon, Hong Kong SAR, China

[4]School of Nursing, Faculty of Health and Social Sciences, Hong Kong Polytechnic University, Hung Hom, Kowloon, Hong Kong SAR, China

[5]State Key Laboratory of Brain and Cognitive Sciences, The University of Hong Kong, Hong Kong SAR, China

Correspondence:

Dr. Raymond Chuen-Chung CHANG, Rm L4-49, Laboratory Block, School of Biomedical Sciences, LKS Faculty of Medicine, Faculty of Medicine Building, 21 Sassoon Road, Pokfulam, Hong Kong SAR, CHINA

E-mail: rccchang@hku.hk Tel: +852 39179127 Fax: +852 28170857

Or

Dr. Wai-Yin CHENG, TU 510, Department of Food Science and Nutrition, The Hong Kong Polytechnic University, Hung Hom, Kowloon, Hong Kong SAR, CHINA

E-mail: wai-yin-nano.cheng@polyu.edu.hk Tel: +852 34008786

Abstract

Background: Increasing lines of evidence have shown that systemic inflammation may contribute to neuroinflammation and accelerate the progression of neurodegenerative diseases. The double-stranded RNA-dependent protein kinase (PKR) is a key signaling molecule that regulates immune responses by regulating macrophage activation, various inflammatory pathways, and the formation of inflammasomes. This study aims to study the role of PKR in regulating systemic inflammation-triggered neuroinflammation and cognitive dysfunctions.

Methods: In this three-part study, laparotomy was used as an experimental model to study neuroimmune responses triggered by systemic inflammation. In the first part, wild-type C57BL/6J and C57BL/6-Tg(CD68-EGFP)1Drg/J mice were randomly assigned to laparotomy under sevoflurane anesthesia or sevoflurane anesthesia alone as a control. The effects of systemic inflammation on neuroinflammation and cognitive function were examined. In the second part, $PKR^{-/-}$ mice were used to determine the role of PKR in regulating laparotomy-induced systemic inflammation, neuroinflammation and cognitive dysfunctions. For the third part, rAAV-DIO-PKR-K296R was injected intracerebroventricularly into the right lateral ventricle of ChAT-IRES-Cre-eGFP mice to inhibit PKR activation in cholinergic neurons. The effects of blocking PKR in cholinergic neurons on modulating glucose metabolism and cognition in the laparotomy model were examined.

Results: Genetic deletion of PKR in mice potently ameliorated the laparotomy-induced peripheral and neural inflammatory responses (downregulated pro-inflammatory cytokine expressions and activation of microglia), and cognitive dysfunctions. Inhibition of PKR in cholinergic neurons in mice could rescue the laparotomy-induced brain glucose hypometabolism and cognitive deficits.

Conclusions: Our results suggested the critical role of PKR on modulating neuroinflammation and cognitive dysfunctions in a peripheral inflammation model. PKR could be a pharmacological target for treating systemic inflammation-induced neuroinflammation and cognitive deficits.

Keywords

Alzheimer's disease; Laparotomy; Macrophage; Microglia; Neuroinflammation; Protein kinase R; Systemic inflammation

Background

Recent studies have shown that systemic inflammation may contribute to neuroinflammation and accelerate the progression of neurodegenerative diseases [1-3]. Neuroinflammation contributes to neurodegenerative disorders including Alzheimer's disease (AD) [4], Parkinson's disease (PD) [5] and amyotrophic lateral sclerosis (ALS) [6]. During systemic inflammation, both the infiltration of circulating cytokines and macrophages into the brain can activate microglia [7, 8]. Activated microglia release pro-inflammatory cytokines, leading to neuronal injury and death [9]. These inflammatory mediators can further facilitate the recruitment of leukocyte into the brain, and perpetuating neuroinflammation [10].

In this study, a non-bacterial endotoxin mouse model of laparotomy is adopted to address the systemic inflammation triggered by surgery. The laparotomy model is applicable to study the perioperative neurocognitive disorders (PND) [11]. Laparotomy [12], as a surgical model, outperforms other experimental models including the tibial fracture surgery [13-15] and injection of bacteria [16] or lipopolysaccharide (LPS) [17] for studying peripheral inflammation, as it allows for a longer period of observation up to 2 weeks [16, 17]. Therefore, the laparotomy model is appropriate for the investigation of whether and how neuroinflammation leads to cognitive dysfunctions upon systemic inflammation.

Double-stranded RNA-dependent protein kinase (PKR), which is a serine/threonine kinase encoded in humans by the EIF2AK2 gene, plays a critical role in regulating mRNA translation, transcription, proliferation, and apoptosis [18]. PKR is a key signaling molecule that modulates immune responses by regulating activation of macrophages [19], various inflammatory pathways, and the formation of inflammasomes [20]; in addition to its established antiviral role. PKR can be activated by various stimuli including cytokines, double-stranded RNA (dsRNA) produced by virus, bacterial LPS, and growth factors [20]. Activation of PKR could regulate the activation of various critical inflammatory kinases including mitogen-activated protein kinases (MAPKs) [21] and inhibitor of nuclear factor-κB (IκB) kinase (IKK) [22]. Furthermore, PKR plays an important role for activation

of inflammasomes and regulating the release of inflammasome-dependent cytokines [23, 24]. Therefore, PKR is critical in regulating inflammatory responses.

In addition to the regulation of immune responses, PKR also plays an essential role in cognition and age-related neurodegenerative diseases. Our laboratory was among the first to reveal that activation of PKR and phosphorylation of eukaryotic initiation factor-2alpha (eIF2α) were implicated in neuronal apoptosis [25]. Overexpression of wild-type PKR in human neuroblastoma cells enhanced the apoptosis induced by β-amyloid peptides, while overexpression of dominant-negative PKR could attenuate the induced apoptosis. Primary cultured neurons from PKR knockout mice showed greater tolerance to β-amyloid peptide neurotoxicity when comparing to the wild-type counterpart [25]. Besides, knockout of PKR could result in enhanced late phase of long-lasting synaptic potentiation in hippocampal slices, increased network excitability and improved cognitive functions with the enhancement of learning and memory in mice [26]. Accordingly, these studies suggested the role of PKR in modulating cognitive functions and neurodegeneration.

With respect to the dual functions of PKR in modulating immune responses and cognition, we hypothesize that PKR regulates the transduction of systemic inflammation into neuroinflammation, and PKR in cholinergic neurons can modulate cognitive functions. We aim to investigate whether PKR can be a pharmacological target for preventing both systemic inflammation-triggered neuroinflammation and systemic inflammation-induced cognitive dysfunctions.

Methods

Animal husbandry

Male wild-type C57BL/6J, C57BL/6-Tg(CD68-EGFP)1Drg/J, PKR$^{-/-}$ and ChAT-IRES-Cre-eGFP mice (3 months) were obtained from the Centre for Comparative Medicine Research (CCMR) of the University of Hong Kong, which is fully accredited by the Association for Assessment and Accreditation of Laboratory Animal Care (AAALAC). Mice were housed in cages under controlled temperature (20 – 22°C), humidity (50 – 60%) and light conditions (12 h:12 h light: dark cycle), with

115 ad libitum access to food and water. Mice were acclimated to the environment for one week before the
116 experiment. All experiments were approved by the Department of Health of the Hong Kong SAR
117 government and the Committee on the Use of Live Animals in Teaching and Research (CULATR) of
118 the University of Hong Kong.

119

120 *Experimental protocols*

121 A non-bacterial endotoxin mouse model of laparotomy is adopted to address the systemic
122 inflammation triggered by surgery. The experimental workflow is summarized in Fig. S1. For the first
123 part of our study, both male wild-type C57BL/6J and C57BL/6-Tg(CD68-EGFP)1Drg/J mice were
124 assigned into 2 groups randomly: laparotomy under sevoflurane anesthesia and control group under
125 sevoflurane anesthesia. In the second part, $PKR^{-/-}$ mice were exposed to laparotomy with sevoflurane
126 anesthesia or sevoflurane anesthesia to examine the role of PKR in regulating systemic inflammation-
127 triggered neuroinflammation. For the third part, intracerebroventricular injection of rAAV-DIO-PKR-
128 K296R into the right lateral ventricle of ChAT-IRES-Cre-eGFP mice was performed to inhibit PKR
129 activation in cholinergic neurons. Mice were then subjected to laparotomy with sevoflurane or
130 sevoflurane anesthesia respectively. The effects of blocking PKR in cholinergic neurons on modulating
131 glucose metabolism and cognitive functions were examined in an inflammatory context.

132

133 *Laparotomy*

134 To induce anesthesia, the animal was placed in a chamber with 5% sevoflurane (Sevorane™, Abbott,
135 Switzerland) and transferred to a nose mask with anesthesia maintained at 3% sevoflurane with a gas
136 flow of 800 ml/min using an inhalation anesthesia machine (Harvard, US). The surgical procedure was
137 performed as described previously with slight modifications [12]. Hair was removed from the surgical
138 site, and the skin was disinfected. A 2.5 cm longitudinal midline incision was made at 0.5 cm below
139 the lower right rib. Approximately 10 cm of the intestine was then exteriorized and rubbed for 2 min
140 before being placed back into the abdominal cavity. 5-0 vicryl and nylon suture (Ethicon, USA) were
141 used for abdominal muscle and skin suture.

142

143 *Stereotaxic injection*

144 Intraperitoneal injection of a ketamine (80 mg/kg) and xylazine (8 mg/kg) mixture was performed to
145 induce anesthesia in the mouse. Prior to surgery, hair was removed from the surgical site, and the skin
146 was disinfected. The head of the animal was then fixed onto the stereotaxic frame (Narishige Scientific
147 Instruments Lab, Japan). Around a 1.5 cm straight midline incision was made to expose the skull.
148 Either rAAV-DIO-PKR-K296R (packaged in AAV serotype 6) (2 μl; 1×10^{13} vg/mL) or 0.9% saline
149 was injected intracerebroventricularly using the Hamilton syringe with a 33-gauge needle (7803-05,
150 Hamilton Company, USA) into the right lateral ventricle (antero-posterior (AP): −0.6 mm, medial-
151 lateral (ML): −1.3 mm, dorsal-ventral (DV): −3.1 mm), at a flow rate of 0.5 μL/min. Following
152 injection, the needle was kept in situ for 5 min to allow for diffusion and avoid solution backflow. A
153 non-absorbable nylon suture (5-0, PS-2; Ethicon, USA) was used to seal the incision site.

154

155 *Behavioral tests*

156 A series of behavioral tests were performed including open field test (OFT), novel object recognition
157 test (NOR), spontaneous alternation Y-maze (SYM) test and puzzle box test (Table S1). Detailed
158 protocols were described in the Supplementary Methods.

159

160 *RNA isolation and quantitative real-time RT-PCR*

161 Mice were sacrificed by CO_2 asphyxiation and decapitation in accordance with the American
162 Veterinary Medical Association (AVMA) guidelines. Animals were then transcardially perfused with
163 ice-cold 0.9% saline. Frontal cortex, hippocampus and liver were collected, snap-frozen and stored at
164 -80°C. Total RNA was extracted from the tissue samples using RNAiso Plus (TAKARA, Japan).
165 Detailed protocols are described in Supplementary Methods. Real-time quantitative PCR was
166 performed with TB Green® Premix Ex Taq™ II (TAKARA, Japan) using a Bio-Rad CFX 96 real-time
167 PCR detection system (Bio-Rad, USA) in triplicate. Sequences of primers are listed in Table S2.

168 Relative expression levels were determined using the comparative CT method to normalize target gene
169 mRNA to GAPDH.

170

171 *Immunohistochemical staining and confocal microscopy*

172 The cryosection preparation processes were described in the Supplementary Methods and were similar
173 to those described previously for human brain sections [27]. Brain sections were blocked with 10%
174 normal goat serum, and then incubated with primary antibodies listed in Table S3 at 4°C overnight,
175 followed by staining with corresponding secondary antibodies (Alexa Fluor, 1:400, Invitrogen, USA)
176 for 1 h at room temperature, and co-staining with 4', 6-diamidino-2-phenylindole (DAPI). Confocal
177 images were acquired by a confocal laser scanning microscope (LSM800; Carl Zeiss, Germany) using
178 Zen Blue software with parameters described in the Supplementary Methods. Quantification of the
179 confocal images was performed using ImageJ software (National Institute of Health, USA).

180

181 *Flow cytometry*

182 Mouse frontal cortex and hippocampus of the C57BL/6-Tg(CD68-EGFP)1Drg/J mice were collected
183 and then homogenized and filtered to obtain the single-cell suspensions, which were then stained with
184 DAPI. Detailed protocol was described in the Supplementary Methods. Cellular fluorescence was
185 measured using an Agilent NovoCyte Quanteon analyzer (Agilent, USA).

186

187 *Targeted metabolomic by GC-MS/MS*

188 Samples were prepared from the frontal cortex collected and detailed preparation protocol were
189 described in the Supplementary Methods. Targeted metabolomics on central carbon metabolism was
190 analyzed using gas chromatography-tandem mass spectrometry (GC-MS/MS). GC-MS/MS analysis
191 was performed on Agilent 7890B GC-Agilent 7010 Triple Quadrupole Mass Spectrometer system
192 (Agilent, USA), with experimental parameters stated in the Supplementary Methods.

193

Statistical analysis

Unless otherwise specified, all statistical analyses were performed on GraphPad Prism v8.0c (GraphPad Software, La Jolla, CA, USA). Data were expressed as means ± SEM. Normality of the data were assessed using the D'Agostino-Pearson normality test. To determine the statistical significance of treatment effects, unpaired two-tailed Student's t-test at $p < 0.05$ was applied for comparing two groups. Interactions between mouse strain and treatment were assessed using two-way ANOVA with Bonferroni post hoc test. Statistical significance was determined if $p < 0.05$.

Results

Laparotomy induced both peripheral and neural inflammation in the wild-type mice

At 4 h following laparotomy, significant increase of IL-1β and monocyte chemoattractant protein (MCP)-1 mRNA expressions were observed in the liver of the laparotomy group when compared to the control counterpart (Fig. 1a). The expression of IL-1β was also significantly upregulated in the hippocampus following laparotomy (Fig. 1a). On postoperative day (POD) 1, there were no significant differences of IL-1β, IL-6, TNF-α and MCP-1 mRNA expression in the liver when compared both the laparotomy and control group (Fig. 1b), suggesting transient systemic inflammation. However, laparotomy significantly increased IL-1β and IL-6 expression in the frontal cortex and hippocampus when compared to the control (Fig. 1b), indicating the ongoing, persistent neuroimmune responses.

To further study the effects of laparotomy on neuroinflammation, we utilized a transgenic C57BL/6-Tg(CD68-EGFP)1Drg/J mouse strain for visualizing the microglia/ macrophage dynamics. C57BL/6-Tg(CD68-EGFP)1Drg/J mice express high levels of enhanced green fluorescent protein (eGFP) in macrophage and activated microglia, aiding in identifying activated microglia and macrophages. Brain sections were immunostained with antibodies against eGFP, TMEM119 (transmembrane protein 119: a microglia-specific marker) and CD105 (endoglin: a vascular endothelial marker). On POD 14, more CD68-EGFP positive cells were observed in both the frontal cortex and hippocampus including cornu ammonis (CA)1, CA3 and dentate gyrus (DG) of the laparotomy group compared to the control counterpart (Fig. S2, S3). This suggested the activation of

221 microglia/macrophages following the laparotomy. Furthermore, an increased number of vessel-
222 associated macrophages (CD68-eGFP^{+}, TMEM119^{-} cells associated with the blood vessels) in the
223 frontal cortex was detected following laparotomy (Fig. S2a, b). Flow cytometry also revealed a notable
224 increase in the number of CD68-eGFP positive cells in both the frontal cortex and the hippocampus
225 on POD 14 when compared to the control counterpart (Fig. 1c–f), suggesting laparotomy induced
226 activation of microglia/macrophages within the brain.

227 To further confirm whether laparotomy induced microglial activation, brain sections from the
228 C57BL/6-Tg(CD68-EGFP)1Drg/J mice were immunostained with a microglial activation marker,
229 ionized calcium-binding adaptor molecule 1 (Iba1). In both the frontal cortex and hippocampus, more
230 Iba1^{+} cells were observed in the laparotomy group when compared to the control (Fig. 2). Increased
231 fluorescence intensity was also observed in the hippocampus following laparotomy. Microglial
232 morphology, which is an important indicator of neuroinflammation, was further quantified using the
233 skeleton analysis [28]. Reduced total endpoints or/and shorter process length per microglial cell were
234 observed in the frontal cortex, CA1 and DG of the hippocampus of the laparotomy group compared
235 with the control counterpart (Fig. 2b, d and h). This revealed that microglia were de-ramified following
236 the laparotomy.

237

238 *Changes of body weight and cognitive performance in the wild-type mice following laparotomy*

239 Body weights were recorded throughout the experiment. A significant weight loss was
240 observed in the wild-type mice within 6 days after the laparotomy (Fig. 3a). Thereafter, no significant
241 weight loss was observed afterwards in the laparotomy group.

242 To study whether laparotomy affects cognitive functions in the wild-type mice, a series of
243 behavioral tests were performed. In the OFT, no significant difference was observed in the total
244 distance travelled and exploration time spent in the central area between the laparotomy group and the
245 control counterpart (Fig. 3b, c). This implied that laparotomy did not affect the locomotor and

exploratory activities, and anxiety level of the mice. The NOR test was then performed to assess recognition memory in mice, based on rodent's innate preference for novelty [29]. On the first day of the NOR, mice from the laparotomy group and the control group spent similar amounts of time for exploring the identical objects (Fig. 3d). On day 2 of the NOR, impaired recognition memory with lower discrimination index was observed in the laparotomy group when compared with the control (Fig. 3e). Moreover, with similar total number of entries (Fig. 3f), impaired spatial working memory, as indicated by reduced percentage of alternation, was observed in the laparotomy group in the SYM test when compared with the control (Fig. 3g). Besides, the puzzle box test was adopted to examine rodent's native problem-solving ability (Trial (T)2, T5, T8 and T11), short-term (T3, T6, T9 and T12) and long-term memory (T4, T7, T10 and T13) [29]. In the habituation task (T1), both group of mice spent similar time to complete the escape task (Fig. 3h). Impaired problem-solving abilities were observed in the laparotomy group which required a longer period of time to complete the escape task in T2, T5 and T11 when compared with the control (Fig. 3i). Furthermore, reduced short-term memory (with increased latency in T12) (Fig. 3j) and long-term memory (with increased latency in T7, T10 and T13) were observed in the laparotomy group compared with the control (Fig. 3k).

Knockout of PKR in mice potently downregulated the increased pro-inflammatory cytokine expressions induced by laparotomy and ameliorated the activation of microglia following laparotomy

Since PKR plays an essential role in regulation of immune responses, we assessed whether genetic deletion of PKR could abrogate laparotomy-induced inflammation. Significant elevation of IL-1β expression was observed in the liver and hippocampus of the wild-type mice at 4 h after laparotomy; but not in the $PKR^{-/-}$ mice after the surgery compared to the control (Fig. 4a). Meanwhile, there was a significant reduction in the IL-1β expression in the liver and frontal cortex of the $PKR^{-/-}$ laparotomy group compared to the wild-type laparotomy group (Fig. 4a). When considering the MCP-1 expression in the liver, a significant increase was observed in the wild-type mice after the laparotomy, but not in the $PKR^{-/-}$ mice (Fig. 4a). Surprisingly, a significant increase was detected in the TNF-α expression in

272 the liver of the PKR$^{-/-}$ laparotomy group when compared to the PKR$^{-/-}$ control (Fig. 4a), which was not
273 observed in the wild-type counterpart.

274 On POD 1, substantial increases in both IL-1β and IL-6 mRNA expression in the frontal cortex
275 and hippocampus of the wild-type laparotomy group were detected when compared to the wild-type
276 control group (Fig. 4b); while no such increases were observed in the PKR$^{-/-}$ mice laparotomy group.
277 Meanwhile, there was a significant reduction in the IL-6 expression in the frontal cortex of the PKR$^{-/-}$
278 laparotomy group compared to the wild-type laparotomy group (Fig. 4b). Furthermore, when
279 comparing the surgical group to the control group for both strains of mice, no significant differences
280 in IL-1β, IL-6, MCP-1, and TNF-α mRNA expression were observed in the liver (Fig. 4b); and no
281 significant alterations in MCP-1, and TNF-α mRNA expression in both the frontal cortex and
282 hippocampus (Fig. 4b).

283 We then further investigated whether knockout of PKR could inhibit activation of microglia in
284 the laparotomy model. When compared the PKR$^{-/-}$ laparotomy group with its control, no observable
285 difference was detected in both the number and fluorescence intensity of Iba1^{+} cells in the frontal
286 cortex (Fig. 5a, b) and hippocampus (CA1, CA3 and DG) (Fig. 5c–h). Concurrently, laparotomy did
287 not induce morphological change (total number of endpoints and summed branch lengths) in microglia
288 in both the frontal cortex (Fig. 5a and b) and hippocampus (Fig. 5c–h) of the PKR$^{-/-}$ mice compared
289 with the control. PKR-/- mice showed ameliorated neuroimmune responses compared to wild-type
290 mice, suggesting its role in regulating neuroinflammation in response to systemic inflammation.

291

292 *Genetic deletion of PKR in mice ameliorated the cognitive impairment induced by laparotomy*

293 Regardless of the mouse strain, laparotomy resulted in a considerable body weight loss within 3 days
294 (Fig. 6a). The body weight of the PKR$^{-/-}$ mice restored to normal (on day 6) earlier than that of the
295 wild-type mice (on day 9). In the laparotomy group, neither strain of mice lost significantly of weight
296 after day 9 (Fig. 6a). Laparotomy did not affect locomotor activity (total distance travelled) and the

297 anxiety level (central duration) of the PKR$^{-/-}$ mice (Fig. 6b, c). On the first day of the NOR test, both
298 strains of mice spent the same time exploring the identical objects (Fig. 6d). On the second day of the
299 NOR, one of the identical objects was being replaced by a novel object. Laparotomy impaired the
300 recognition memory (lower discrimination index) of the wild-type mice (Fig. 6e); but not in the PKR^{-}
301 $^{/-}$ mice. In the SYM test, laparotomy impaired spatial recognition memory (reduced percentage of
302 alternation) of the wild-type mice, but not the PKR$^{-/-}$ mice (Fig. 6g). No significant difference was
303 observed in the total number of entries between the surgery and the control (Fig. 6f).

304 To further assess rodent's problem-solving skill, short-term and long-term memory, the puzzle
305 box test was conducted. Throughout habituation, there was no significant difference between the
306 laparotomy and control groups, regardless of mouse strain (Fig. 6h). When comparing the mouse
307 strains, the PKR$^{-/-}$ mice demonstrated greater latency to reach the goal zone than the wild-type mice
308 (Fig. 6h). Considering the problem-solving ability, the PKR$^{-/-}$ laparotomy mice performed similarly to
309 PKR knockout controls. (Fig. 6i). This differs from the wild-type laparotomy mice which took longer
310 to solve the task T2, T5 and T11 (Fig. 6i). Concurrently, when compared the PKR$^{-/-}$ mice with the
311 wild-type mice, significant differences were also detected in the native problem-solving ability (Fig.
312 6i). In T2, the PKR$^{-/-}$ laparotomy mice demonstrated greater latency when compared with the wild-
313 type laparotomy group (Fig. 6i); and a similar trend was also detected in the T11 when comparing the
314 PKR$^{-/-}$ control and the wild-type control counterpart (Fig. 6i). Furthermore, laparotomy did not impair
315 the short-term memory and long-term memory in the PKR$^{-/-}$ mice, while the wild-type laparotomy
316 group showed significant impairment (Fig. 6j, k). This suggested that genetic deletion of PKR could
317 ameliorate the cognitive deficits induced by laparotomy.

318

319 *Inhibition of PKR in cholinergic neurons ameliorated laparotomy-induced cognitive dysfunctions*

320 To inhibit the activation of PKR in cholinergic neurons, intracerebroventricular injection of rAAV-
321 DIO-PKR-K296R into the right lateral ventricle of ChAT-IRES-Cre-eGFP mice was performed. The
322 rAAV expresses a dominant negative form of the PKR, PKR-K296R, under the regulation of a double-

323 floxed inverse orientation (DIO) switch (Fig. S4a). At 4 weeks after the stereotaxic injection of the
324 rAAV-DIO-PKR-K296R, both reduced fluorescence intensity of the p-PKR (T446) signal and
325 fluorescence ratio of p-PKR to the eGFP signal were detected in the rAAV-DIO-PKR-K296R-treated
326 group when compared with the saline-treated control (Fig. S4b, c). Therefore, in ChAT-IRES-Cre-
327 eGFP mice, the expression of the dominant-negative form of PKR-K296R effectively suppressed the
328 activation (phosphorylation) of PKR.

329 At 4 weeks following stereotaxic injection, mice were divided into four groups including: the
330 saline-treated control group given only sevoflurane (SAL-CON), the saline-treated group subjected to
331 laparotomy (SAL-LAP), the AAV-treated group given only sevoflurane (AAV-CON) and the AAV-
332 treated group subjected to laparotomy (AAV-LAP). Within 3 days after laparotomy, both the SAL-
333 LAP and AAV-LAP lost significant weight, similar to the wild-type and PKR-KO mice (Fig. 7a). On
334 POD 6, body weight returned to normal; with no significant difference among all the groups (Fig. 7a).

335 To investigate the effects of inhibiting PKR in cholinergic neurons on cognitive functions in
336 the inflammatory context, different behavioral tests were performed. Fig. 7b and c showed that
337 injection of rAAV-DIO-PKR-K296R and laparotomy did not affect locomotor activity (total distance
338 travelled) and anxiety level (central duration). In the SYM test, impaired spatial memory with lower
339 percentage of alternation was detected in the SAL-LAP when compared to the SAL-CON (Fig. 7e);
340 while not in the AAV-treated group. No significant difference was observed in the total number of
341 entries among all the groups (Fig. 7d). Our findings suggested that inhibition of PKR in cholinergic
342 neurons could alleviate the laparotomy-induced impairment of spatial working memory.

343 Regarding the puzzle box test, in the habituation task (T1), all groups of mice completed the
344 escape task in about the same amount of time (Fig. 7f). Considering the problem-solving ability,
345 contrasting behaviors were observed. In the T2 task, the SAL-LAP demonstrated increased latency
346 when compared with the SAL-CON (Fig. 7g); whereas no significant difference was observed between
347 the AAV-treated group (Fig. 7g). Meanwhile, the AAV-LAP solved the T2 task faster than the SAL-
348 LAP (Fig. 7g). This revealed that inhibiting PKR in cholinergic neurons could improve the cognitive

349 functions of mice in the T2 task following laparotomy. In the T5 and T8 task, however, both AAV-
350 treated and saline-treated mice showed increased latency time following laparotomy than their control
351 (Fig. 7g). With respect to T11 task, the AAV-LAP demonstrated a significant increase in latency when
352 compared to the AAV-CON (Fig. 7g). Meanwhile, for the T11 task, the AAV-CON demonstrated a
353 better problem-solving skill than the SAL-CON (Fig. 7g).

354 Regarding the short-term memory, consistent results were observed in both the T3 and T6 tasks
355 (Fig. 7h). The SAL-LAP demonstrated impaired short-term memory, with increased latency detected
356 to solve the T3 and T6 tasks, as compared to the SAL-CON (Fig. 7h); while such kind of differences
357 were not detected in the AAV-treated groups. Additionally, in the T3 task, the AAV-LAP escaped
358 faster than the SAL-LAP (Fig. 7h). It indicated that inhibiting PKR in cholinergic neurons helped to
359 alleviate the short-term memory deficits induced by laparotomy. However, for the T9 task, both AAV-
360 treated and saline-treated mice showed increased latency following laparotomy than their control
361 groups (Fig. 7h). Furthermore, the AAV-treated groups demonstrated a reduction in latency for the
362 T12 task compared to its saline-treated counterpart (Fig. 7h). Therefore, inhibition of PKR in
363 cholinergic neurons could improve short-term memory.

364 Considering the long-term memory, contrasting behaviors were observed in the T4 and T7
365 tasks, with the SAL-LAP showing impairment in the T4 task, while the AAV rescued it (Fig. 7i). The
366 T7 task showed a noticeable change only in the AAV-treated groups, not in the saline-treated groups
367 (Fig. 7i). No significant difference was observed between the AAV-treated groups and the SAL-treated
368 groups for all the tasks testing long-term memory (T4, T7, T10 and T13 tasks). Therefore, no concrete
369 conclusions concerning the influence of PKR inhibition in cholinergic neurons on long-term memory
370 could be drawn.

371

372 *Inhibition of PKR in cholinergic neurons alters glucose metabolism in the frontal cortex in a*
373 *laparotomy model*

To examine the impact of PKR inhibition in cholinergic neurons on brain glucose metabolism, MS-based targeted metabolomics was performed. Distinct clustering was observed between the SAL-LAP and AAV-CON (a, b). The heatmap depicted the changes of quantified metabolites including tricarboxylic acids and glycolysis intermediates in the frontal cortex across all the groups (Fig. 8c). Laparotomy significantly reduced the level of phosphoenolpyruvate in the SAL-LAP compared with its control (Fig. 8e). However, no significant difference in the phosphoenolpyruvate level was observed in the AAV-treated group following laparotomy. Inhibiting PKR in cholinergic neurons could ameliorate the laparotomy-induced changes in the phosphoenolpyruvate level. Similarly, laparotomy lowered the succinate level in the SAL-treated group (Fig. 8f); while not in the AAV-treated group (Fig. 8f). No significant difference in glucose levels was detected among all the groups (Fig. 8d). Apart from the laparotomy-induced changes in the glycolysis intermediates, inhibition of PKR in cholinergic neurons significantly elevated the level of 6-phosphogluconate in the AAV-CON compared with the SAL-CON (Fig. 8g), suggesting that inhibition of PKR in cholinergic neurons could alter brain energy metabolism.

Discussion

Neuroinflammation is a major cause of cognitive impairment in PND. Here, we employed a clinically relevant mouse model of laparotomy to induce both peripheral and neural inflammation; and further demonstrate the regulatory role of PKR on systemic inflammation-induced neuroinflammation and cognitive dysfunctions.

Considering the laparotomy model, both the systemic and neuro-immune responses developed rapidly after the surgery. Theoretically, laparotomy resulted in peritoneal air exposure [30, 31], tissue injury and damage of the intestinal mucosa barrier, leading to increased inflammatory mediators and the translocation of gut bacteria and endotoxin from the gut to the systemic circulation, contributing to systemic inflammation [32]. Our study observed significant increase of the mRNA expression for cytokines in both the liver (IL-1β and MCP-1) and brain tissues (IL-1β) at 4 h after laparotomy (Fig. 1a). On POD 1, laparotomy triggered a significant upregulation of both the IL-1β and IL-6 mRNA

expression in the hippocampus (Fig. 1b). IL-1β is a key mediator in driving neuroinflammation and contributes to the pathogenesis of AD [33] and PD [34]. Through activation of the nuclear factor κB (NF-κB), IL-1β can induce the expression of various proinflammatory cytokines including IL-6 and TNF-α [35]. This may partially explain the increase of the IL-6 expression of the laparotomy group on POD 1 (Fig. 1b). However, the induced systemic inflammation is relatively transient, with the proinflammatory cytokine expression level in the liver returned to normal on POD 1 (Fig. 1b). Therefore, a transient systemic inflammation is already sufficient to induce neuroinflammation, as evident by the persistent microgliosis revealed by both the flow cytometry (Fig. 1c–f) and confocal imaging (Fig. 2) on POD 14. Our findings are also consistent with a prior study that demonstrated significant activation of microglia in both frontal cortex and hippocampus were observed after laparotomy [12]. In addition to activation of microglia, cognitive deficits (Fig. 3) were also detected in the laparotomy model in the wild-type mice. Taken together, the laparotomy model is a viable and relevant paradigm for studying systemic inflammation-triggered neuroinflammation and cognitive dysfunction.

Our study is the first to show that genetic deletion of PKR could alleviate both laparotomy-induced peripheral and neural inflammation, with potent downregulation of the increased expression of IL-1β and IL-6 in the liver, frontal cortex and hippocampus following laparotomy (Fig. 4a and b). Indeed, PKR is involved in the activation of IL-1b. Therefore, knockout of PKR can help prevent the cleavage of pro-IL-1b to IL-1b. These findings were consistent with other previous studies showing that PKR could attenuate inflammation by regulating inflammasome activation [36] and various inflammatory pathways including TNF [37], p38 MAPK [21] and NF-κB/IκB signaling pathway [38]. Inhibition of PKR could prevent the activation of IκB and NF-κB and reduce the production of IL-1β in both primary murine mixed neuron-astrocyte-microglia co-culture model [38], and RAW264.7 macrophages [39]. Subsequently, reduced IL-1β further downregulate the expression of IL-6 through preventing the activation of NF-κB. Intriguingly, at 4 h after the surgery, a significant increase was observed in the expression of TNF-α in the liver of the $PKR^{-/-}$ laparotomy group but not in the wild-type counterpart (Fig. 4a). However, no significant difference was observed between the $PKR^{-/-}$ laparotomy and the wild-type laparotomy group. Similar findings were also observed in our previous

429 study which demonstrated a significant increase in the expression of TNF-α in the hippocampus of the
430 $PKR^{-/-}$ mice after *E. coli* challenge but not in the wild-type control counterpart [16]. Indeed, PKR is
431 required for TNF-dependent activation of NF-kB, c-Jun N-terminal kinase (JNK) and protein kinase
432 B (Akt). Genetic deletion of PKR could abrogate the TNF-induced activation of the above signaling
433 pathways. Therefore, it is speculated that $PKR^{-/-}$ laparotomy mice may tend to express more TNF-α in
434 order to activate the downstream pathways. Besides, knockout of PKR in mice could suppress
435 laparotomy-induced activation of microglia in both the frontal cortex and the hippocampus (Fig. 5).
436 Our findings were aligned with a previous study showing that genetic deletion of PKR in mice could
437 prevent activation of microglia following the intraperitoneal injection of LPS [40]. Indeed, PKR plays
438 a critical role in regulating the activation of microglia/macrophages. PKR is essential for LPS-induced
439 inducible nitric oxide synthase expression [41], and therefore responsible for the macrophage
440 inflammatory response through regulating the production of a proinflammatory factor, nitric oxide
441 [42]. Moreover, PKR has been found to be necessary for dsRNA-induced activation of macrophage
442 [39]. All the aforementioned studies supported the potential role of PKR on activation of
443 microglia/macrophages. Furthermore, genetic deletion of PKR in mice could rescue the laparotomy-
444 induced impairment of problem-solving ability, spatial working memory, short-term and long-term
445 memory in mice (Fig. 6e, g, i–k).

446 Another novel finding of this project is that inhibition of PKR in cholinergic neurons could
447 modulate cognitive functions in the inflammatory context. The cholinergic system is selected for
448 investigation as it is not only essential for cognition but also plays a vital role in regulating
449 inflammation through the cholinergic anti-inflammatory pathway [43]. This pathway can connect
450 systemic inflammation and neuroinflammation. This would elucidate the neuron-specific effects of
451 PKR on cognition during inflammation beyond its immune regulatory roles. This study has
452 demonstrated that inhibition of the PKR in cholinergic neurons alleviated the laparotomy-induced
453 impairment of short-term and spatial working memory (Fig. 7e and h). Previous studies showed that
454 inhibition of PKR could improve cortex-dependent memory consolidation in both rats and mice [44].
455 $PKR^{-/-}$ mice demonstrated enhanced conditioned taste aversion memory compared with the wild-type
456 control [44]; while activation of PKR could impair hippocampal late-phase LTP and memory

consolidation in the PKR recombinant mice [45]. All the abovementioned studies supported the critical role of PKR on regulating cognitive functions.

We observed that laparotomy could lead to brain glucose hypometabolism with reduction in both the glycolysis and citric acid cycle intermediates (phosphoenolpyruvate and succinate) (Fig. 8), which is a common hallmark of neurodegenerative diseases in the preclinical stages including AD and PD [46, 47]. Progressive reduction of the brain glucose metabolism has been positively correlated with the amyloid load and cognitive decline in mild cognitive impairment, early AD and PD patients [47-49]. Reduced concentrations of glycolytic intermediates, including phosphoenolpyruvate, were observed in the cerebrospinal fluid of AD patients [50]. In contrast, administration of succinate into the brain by retrodialysis could improve the brain reduced/oxidized nicotinamide adenine dinucleotide ($NADH/NAD^+$) redox state [51], and improve brain energy metabolism in traumatic brain injury patients [52]. A close association between brain glucose metabolism and cognition was established in all of the abovementioned studies.

Our study unraveled the novel role of PKR in regulating brain glucose metabolism in the laparotomy model. Blocking PKR in cholinergic neurons could rescue the laparotomy-induced alterations in glucose metabolism in frontal cortex on POD 14 (Fig. 8e and f). Indeed, PKR regulates glucose homeostasis [53] and induces insulin resistance [54, 55]. Increased phosphorylation of eIF2α is a hallmark of insulin resistance and obesity [54-56]. Under metabolic and obesity-induced stress, PKR could form a complex with TAR RNA-binding protein (TRBP), activating JNK [53]. Inhibiting TRBP in the liver could improve insulin resistance and glucose metabolism as well as alleviate inflammation [53]. The interaction between PKR and TRBP has been shown to link metabolism to regulation of inflammatory signaling. Yet, no prior study examined the effect of blocking PKR in brain on glucose metabolism. Our findings supported that PKR in cholinergic neurons play a critical role in modulating glucose metabolism in an inflammatory context. Further study to unveil the underlying regulatory networks is warranted.

Conclusions

484 In summary, the laparotomy model was a stable and viable model for studying neuroimmune
485 responses triggered by systemic inflammation, as evidenced by microgliosis and cognitive
486 dysfunction. By genetic deletion of PKR, we demonstrated the critical role of PKR in regulating both
487 the peripheral and neural inflammation. Knockout of PKR could help alleviate neuroimmune responses
488 and cognitive impairment induced by laparotomy. Furthermore, inhibition of PKR in cholinergic
489 neurons of the laparotomy mice demonstrated a neuroprotective role, with improved glucose
490 metabolism and cognitive functions in the inflammatory context. Based on our combined findings,
491 PKR could be a pharmacological target for treating systemic inflammation-induced
492 neuroinflammation and cognitive deficits.

493

494 **List of abbreviations**

495 AAALAC: Association for Assessment and Accreditation of Laboratory Animal Care

496 AAV-CON: The AAV-treated group given only sevoflurane

497 AAV-LAP: The AAV-treated group subjected to laparotomy

498 AD: Alzheimer's disease

499 Akt: Protein kinase B

500 ALS: Amyotrophic lateral sclerosis

501 AP: Antero-posterior

502 CA: Cornu ammonis

503 CCMR: Centre for Comparative Medicine Research

504 DAPI: 4', 6-Diamidino-2-phenylindole.

505 DG: Dentate gyrus

506 DIO: Double-floxed inverse orientation

507 dsRNA: Double-stranded RNA

508 DV: dorsal-ventral

509 eGFP: Enhanced green fluorescent protein

510 eIF2α: Eukaryotic initiation factor-2alpha

511 GC-MS/MS: Gas chromatography-tandem mass spectrometry

512 Iba1: Ionized calcium-binding adaptor molecule 1

513 IKK: Inhibitor of nuclear factor-κB kinase

514 JNK: c-Jun N-terminal kinase

515 LPS: Lipopolysaccharide

516 MAPKs: Mitogen-activated protein kinases

517 MCP: Monocyte chemoattractant protein

518 ML: Medial-lateral

519 NF-κB: Nuclear factor κB

520 NOR: Novel object recognition test

521 OFT: Open field test

522 PD: Parkinson's disease

523 PKR: Double-stranded RNA-dependent protein kinase

524 PND: Perioperative neurocognitive disorders

525 POD: Postoperative day

526 SAL-CON: The saline-treated control group given only sevoflurane

527 SAL-LAP: The saline-treated group subjected to laparotomy

528 SYM: Spontaneous alternation Y-maze test

529 TMEM119: Transmembrane protein 119

530 TRBP: TAR RNA-binding protein

Declarations

Ethics approval and consent to participate

All experiments were approved by the Department of Health of the Hong Kong SAR government and the CULATR of the University of Hong Kong.

Consent for publication

Not applicable.

Availability of data and materials

The online version contains supplementary material. All raw data are available at the HKU data repository.

Competing interests

Authors declare no competing interests.

Funding

The study is supported by General Research Fund (17123217).

Authors' contributions

WYC conducted experiments, performed data analyses, and wrote the manuscript. XZL helped with the animal handling and experiments. MSLL contributed to part of the confocal imaging. WYC and RCCC worked on experimental design. RCCC conceived the idea, supervised the study, provided funding, and revised the manuscript. All authors read and approved the final manuscript.

Acknowledgements

We appreciate Mr. Justin Man Hin Wong's assistance in experiments, and staffs from CCMR for animal experiments, and Centre for PanorOmic Sciences for guidance on confocal imaging and flow cytometry.

References

1. Hoogland I, Houbolt C, van Westerloo DJ, van Gool WA, van de Beek D. Systemic inflammation and microglial activation: systematic review of animal experiments. Journal of neuroinflammation. 2015;12(1):1-13.

2. Lopez-Rodriguez AB, Hennessy E, Murray CL, Nazmi A, Delaney HJ, Healy D, et al. Acute systemic inflammation exacerbates neuroinflammation in Alzheimer's disease: IL-1β drives amplified responses in primed astrocytes and neuronal network dysfunction. Alzheimer's & Dementia. 2021;17(10):1735-55.
3. Wang RP-H, Ho Y-S, Leung WK, Goto T, Chang RC-C. Systemic inflammation linking chronic periodontitis to cognitive decline. Brain, Behavior, and Immunity. 2019;81:63-73.
4. Heneka MT, Carson MJ, El Khoury J, Landreth GE, Brosseron F, Feinstein DL, et al. Neuroinflammation in Alzheimer's disease. The Lancet Neurology. 2015;14(4):388-405.
5. Hirsch EC, Hunot S. Neuroinflammation in Parkinson's disease: a target for neuroprotection? The Lancet Neurology. 2009;8(4):382-97.
6. Philips T, Robberecht W. Neuroinflammation in amyotrophic lateral sclerosis: role of glial activation in motor neuron disease. The Lancet Neurology. 2011;10(3):253-63.
7. Fu R, Shen Q, Xu P, Luo JJ, Tang Y. Phagocytosis of microglia in the central nervous system diseases. Molecular neurobiology. 2014;49(3):1422-34.
8. Kempuraj D, Thangavel R, Selvakumar GP, Zaheer S, Ahmed ME, Raikwar SP, et al. Brain and Peripheral Atypical Inflammatory Mediators Potentiate Neuroinflammation and Neurodegeneration. Frontiers in Cellular Neuroscience. 2017;11.
9. Streit WJ, Mrak RE, Griffin WST. Microglia and neuroinflammation: a pathological perspective. Journal of neuroinflammation. 2004;1(1):14-.
10. Varvel NH, Neher JJ, Bosch A, Wang W, Ransohoff RM, Miller RJ, et al. Infiltrating monocytes promote brain inflammation and exacerbate neuronal damage after status epilepticus. Proceedings of the National Academy of Sciences. 2016;113(38):E5665.
11. Evered L, Silbert B, Knopman DS, Scott DA, DeKosky ST, Rasmussen LS, et al. Recommendations for the Nomenclature of Cognitive Change Associated with Anaesthesia and Surgery-2018. Anesthesiology. 2018;129(5):872-9.
12. Huang C, Irwin MG, Wong GTC, Chang RCC. Evidence of the impact of systemic inflammation on neuroinflammation from a non-bacterial endotoxin animal model. Journal of Neuroinflammation. 2018;15(1):147.
13. Lu Y, Xu X, Dong R, Sun L, Chen L, Zhang Z, et al. MicroRNA-181b-5p attenuates early postoperative cognitive dysfunction by suppressing hippocampal neuroinflammation in mice. Cytokine. 2019;120:41-53.
14. Xu J, Dong H, Qian Q, Zhang X, Wang Y, Jin W, et al. Astrocyte-derived CCL2 participates in surgery-induced cognitive dysfunction and neuroinflammation via evoking microglia activation. Behavioural Brain Research. 2017;332:145-53.
15. Degos V, Vacas S, Han Z, van Rooijen N, Gressens P, Su H, et al. Depletion of Bone Marrow–derived Macrophages Perturbs the Innate Immune Response to Surgery and Reduces Postoperative Memory Dysfunction. Anesthesiology. 2013;118(3):527-36.
16. Poon DC-H, Ho Y-S, You R, Tse H-L, Chiu K, Chang RC-C. PKR deficiency alters E. coli-induced sickness behaviors but does not exacerbate neuroimmune responses or bacterial load. Journal of Neuroinflammation. 2015;12(1):212.
17. Carret-Rebillat A-S, Pace C, Gourmaud S, Ravasi L, Montagne-Stora S, Longueville S, et al. Neuroinflammation and Aβ Accumulation Linked To Systemic Inflammation Are Decreased By Genetic PKR Down-Regulation. Scientific Reports. 2015;5(1):8489.
18. Garcia M, Meurs E, Esteban M. The dsRNA protein kinase PKR: virus and cell control. Biochimie. 2007;89(6-7):799-811.
19. Maggi LB, Heitmeier MR, Scheuner D, Kaufman RJ, Buller RML, Corbett JA. Potential role of PKR in double-stranded RNA-induced macrophage activation. The EMBO journal. 2000;19(14):3630-8.
20. Williams BRG. Signal Integration via PKR. Science's STKE. 2001;2001(89):re2-re.
21. Goh KC, deVeer MJ, Williams BRG. The protein kinase PKR is required for p38 MAPK activation and the innate immune response to bacterial endotoxin. The EMBO Journal. 2000;19(16):4292-7.
22. Zamanian-Daryoush M, Mogensen TH, DiDonato JA, Williams BRG. NF-κB Activation by Double-Stranded-RNA-Activated Protein Kinase (PKR) Is Mediated through NF-κB-Inducing Kinase and IκB Kinase. Mol Cell Biol. 2000;20(4):1278.
23. Yim HCH, Williams BRG. Protein Kinase R and the Inflammasome. Journal of Interferon & Cytokine Research. 2014;34(6):447-54.

24. Lu B, Nakamura T, Inouye K, Li J, Tang Y, Lundbäck P, et al. Novel role of PKR in inflammasome activation and HMGB1 release. Nature. 2012;488(7413):670-4.
25. Chang RCC, Suen KC, Ma CH, Elyaman W, Ng HK, Hugon J. Involvement of double-stranded RNA-dependent protein kinase and phosphorylation of eukaryotic initiation factor-2α in neuronal degeneration. Journal of neurochemistry. 2002;83(5):1215-25.
26. Zhu Ping J, Huang W, Kalikulov D, Yoo Jong W, Placzek Andon N, Stoica L, et al. Suppression of PKR Promotes Network Excitability and Enhanced Cognition by Interferon-γ-Mediated Disinhibition. Cell. 2011;147(6):1384-96.
27. Chang RC, Suen KC, Ma CH, Elyaman W, Ng HK, Hugon J. Involvement of double-stranded RNA-dependent protein kinase and phosphorylation of eukaryotic initiation factor-2alpha in neuronal degeneration. J Neurochem. 2002;83(5):1215-25.
28. Young K, Morrison H. Quantifying microglia morphology from photomicrographs of immunohistochemistry prepared tissue using ImageJ. JoVE (Journal of Visualized Experiments). 2018(136):e57648.
29. Ho YS, Lau CF, Lee K, Tan JY, Lee J, Yung S, et al. Impact of unilateral ureteral obstruction on cognition and neurodegeneration. Brain Res Bull. 2021;169:112-27.
30. Bao J, Tan S, Yu W, Lin Z, Dong Y, Chen Q, et al. The Effect of Peritoneal Air Exposure on Intestinal Mucosal Barrier. Gastroenterology Research and Practice. 2014;2014:674875.
31. Tan S, Yu W, Lin Z, Chen Q, Shi J, Dong Y, et al. Peritoneal Air Exposure Elicits an Intestinal Inflammation Resulting in Postoperative Ileus. Mediators of Inflammation. 2014;2014:924296.
32. Jacobi CA, Ordemann J, Zieren HU, Volk HD, Bauhofer A, Halle E, et al. Increased Systemic Inflammation After Laparotomy vs Laparoscopy in an Animal Model of Peritonitis. Archives of Surgery. 1998;133(3):258-62.
33. Shaftel SS, Griffin WST, O'Banion MK. The role of interleukin-1 in neuroinflammation and Alzheimer disease: an evolving perspective. Journal of Neuroinflammation. 2008;5(1):7.
34. Saghazadeh A, Ferrari CC, Rezaei N. Deciphering variability in the role of interleukin-1β in Parkinson's disease. Reviews in the Neurosciences. 2016;27(6):635-50.
35. Moynagh PN. The interleukin-1 signalling pathway in astrocytes: a key contributor to inflammation in the brain. J Anat. 2005;207(3):265-9.
36. Lu B, Nakamura T, Inouye K, Li J, Tang Y, Lundbäck P, et al. Novel role of PKR in inflammasome activation and HMGB1 release. Nature. 2012;488(7413):670-4.
37. Takada Y, Ichikawa H, Pataer A, Swisher S, Aggarwal BB. Genetic deletion of PKR abrogates TNF-induced activation of IkappaBalpha kinase, JNK, Akt and cell proliferation but potentiates p44/p42 MAPK and p38 MAPK activation. Oncogene. 2007;26(8):1201-12.
38. Couturier J, Paccalin M, Morel M, Terro F, Milin S, Pontcharraud R, et al. Prevention of the β-amyloid peptide-induced inflammatory process by inhibition of double-stranded RNA-dependent protein kinase in primary murine mixed co-cultures. J Neuroinflammation. 2011;8(1):72.
39. Maggi LB, Jr., Heitmeier MR, Scheuner D, Kaufman RJ, Buller RM, Corbett JA. Potential role of PKR in double-stranded RNA-induced macrophage activation. The EMBO journal. 2000;19(14):3630-8.
40. Carret-Rebillat A-S, Pace C, Gourmaud S, Ravasi L, Montagne-Stora S, Longueville S, et al. Neuroinflammation and Aβ accumulation linked to systemic inflammation are decreased by genetic PKR down-regulation. Scientific Reports. 2015;5(1):1-8.
41. He Y, Franchi L, Núñez G. The protein kinase PKR is critical for LPS-induced iNOS production but dispensable for inflammasome activation in macrophages. European Journal of Immunology. 2013;43(5):1147-52.
42. McNeill E, Crabtree MJ, Sahgal N, Patel J, Chuaiphichai S, Iqbal AJ, et al. Regulation of iNOS function and cellular redox state by macrophage Gch1 reveals specific requirements for tetrahydrobiopterin in NRF2 activation. Free Radic Biol Med. 2015;79:206-16.
43. Rosas-Ballina M, Tracey KJ. Cholinergic control of inflammation. J Intern Med. 2009;265(6):663-79.
44. Stern E, Chinnakkaruppan A, David O, Sonenberg N, Rosenblum K. Blocking the eIF2α Kinase (PKR) Enhances Positive and Negative Forms of Cortex-Dependent Taste Memory. The Journal of Neuroscience. 2013;33(6):2517.

45. Jiang Z, Belforte JE, Lu Y, Yabe Y, Pickel J, Smith CB, et al. eIF2α Phosphorylation-Dependent Translation in CA1 Pyramidal Cells Impairs Hippocampal Memory Consolidation without Affecting General Translation. The Journal of Neuroscience. 2010;30(7):2582.
46. Malkov A, Popova I, Ivanov A, Jang S-S, Yoon SY, Osypov A, et al. Aβ initiates brain hypometabolism, network dysfunction and behavioral abnormalities via NOX2-induced oxidative stress in mice. Communications biology. 2021;4(1):1054.
47. Firbank MJ, Yarnall AJ, Lawson RA, Duncan GW, Khoo TK, Petrides GS, et al. Cerebral glucose metabolism and cognition in newly diagnosed Parkinson's disease: ICICLE-PD study. Journal of Neurology, Neurosurgery & Psychiatry. 2017;88(4):310.
48. Drzezga A, Lautenschlager N, Siebner H, Riemenschneider M, Willoch F, Minoshima S, et al. Cerebral metabolic changes accompanying conversion of mild cognitive impairment into Alzheimer's disease: a PET follow-up study. Eur J Nucl Med Mol Imaging. 2003;30(8):1104-13.
49. Mosconi L, Pupi A, De Leon MJ. Brain glucose hypometabolism and oxidative stress in preclinical Alzheimer's disease. Ann N Y Acad Sci. 2008;1147:180-95.
50. Bergau N, Maul S, Rujescu D, Simm A, Navarrete Santos A. Reduction of Glycolysis Intermediate Concentrations in the Cerebrospinal Fluid of Alzheimer's Disease Patients. Front Neurosci. 2019;13:871-.
51. Stovell MG, Mada MO, Helmy A, Carpenter TA, Thelin EP, Yan J-L, et al. The effect of succinate on brain NADH/NAD+ redox state and high energy phosphate metabolism in acute traumatic brain injury. Scientific Reports. 2018;8(1):11140.
52. Khellaf A, Garcia NM, Tajsic T, Alam A, Stovell MG, Killen MJ, et al. Focally administered succinate improves cerebral metabolism in traumatic brain injury patients with mitochondrial dysfunction. J Cereb Blood Flow Metab. 2022;42(1):39-55.
53. Nakamura T, Kunz RC, Zhang C, Kimura T, Yuan CL, Baccaro B, et al. A critical role for PKR complexes with TRBP in Immunometabolic regulation and eIF2α phosphorylation in obesity. Cell Rep. 2015;11(2):295-307.
54. Nakamura T, Furuhashi M, Li P, Cao H, Tuncman G, Sonenberg N, et al. Double-Stranded RNA-Dependent Protein Kinase Links Pathogen Sensing with Stress and Metabolic Homeostasis. Cell. 2010;140(3):338-48.
55. Carvalho BM, Oliveira AG, Ueno M, Araújo TG, Guadagnini D, Carvalho-Filho MA, et al. Modulation of double-stranded RNA-activated protein kinase in insulin sensitive tissues of obese humans. Obesity (Silver Spring). 2013;21(12):2452-7.
56. Carvalho-Filho MA, Carvalho BM, Oliveira AG, Guadagnini D, Ueno M, Dias MM, et al. Double-stranded RNA-activated protein kinase is a key modulator of insulin sensitivity in physiological conditions and in obesity in mice. Endocrinology. 2012;153(11):5261-74.

Fig. 1. Laparotomy induced both systemic inflammation and neuroinflammation. Relative cytokine mRNA expressions were measured in the liver, frontal cortex, and hippocampus of C57BL/6J mice at (A) 4 h and (B) 1 day after laparotomy. Representative flow cytometry plots illustrating the increase of CD68-eGFP$^+$ cells in the (C) frontal cortex and (E) hippocampus of the CD68-eGFP mice on postoperative day 14. The morphological gating strategy refers to dot plot SSC-H versus FSC-H to eliminate debris and aggregates for the control and laparotomy group in the (C) frontal cortex and (E) hippocampus. Doublets are excluded by plotting FSC-H versus width and SSC-H versus width. The proportion of CD68-eGFP$^+$ cells (labeled with eGFP) and cell viability (labeled with DAPI) were determined by flow cytometry with FITC and pacific blue channel respectively. The data generated are plotted in two-dimensional dot plots in which FITC-A versus Pacific-Blue-A. A four-quadrant gate was established: Q1) live, CD68-eGFP$^+$ cells (FITC positive/Pacific blue negative); Q2) dead, CD68-eGFP$^+$ cells (FITC positive/Pacific blue positive); Q3) live cells without CD68 expression (FITC negative/Pacific blue negative); Q4, dead cells without CD68 expression (FITC negative/Pacific blue positive). The percentage of CD68-eGFP$^+$ cells of the control and laparotomy group in the (D) frontal cortex and (F) hippocampus were plotted. n = 6 per group. Data are expressed as mean ± S.E.M. Differences were assessed by unpaired two-tailed Student's t-test as follows: $^*p < 0.05$ and $^{**}p < 0.01$ compared with the control group.

Fig. 2. Laparotomy induced activation of microglia in frontal cortex and hippocampus after laparotomy. Representative confocal images of the immunohistochemical staining of DAPI, and Iba1 in the (A) frontal cortex, (C) cornu ammonis (CA) 1, (E) CA3 and (G) dentate gyrus (DG) of the hippocampus sections from CD68-eGFP mice of the control and laparotomy group on postoperative day 14. The number of Iba1 positive cells, the relative fluorescence intensity of Iba1 positive cells, the total number of endpoints per Iba1 positive cell, and summed process length per Iba1 positive cell in the (B) frontal cortex, (D) CA 1, (F) CA3 and (H) DG of the hippocampus sections were quantified. n = 5 per group. Data are expressed as mean ± S.E.M. Differences were assessed by unpaired two-tailed Student's t-test denoted as follows: $^*p < 0.05$, $^{**}p < 0.01$ and $^{***}p < 0.001$ compared with the control group.

Fig. 3. Cognitive impairment of C57BL/6J mice following laparotomy. (A) Percentage of the body weight change from baseline of the laparotomy and control group during the postoperative period. (B) Total distance travelled and (C) central duration of mice in the open-field test were measured. (D) Discrimination index, which is the ratio of exploration time of one object to two objects, was measured on the novel object recognition test day 1 (with two identical objects: A+A) and (E) day 2 (with a novel object replaced the familiar one: A+B). (F) Total number of arm entries and (G) percentage of alternation were measured in the spontaneous alternation Y-maze test. In the puzzle box test, the latency time for the mice entering the goal zone in different tasks were measured. All the tasks include (H) task for habituation (T1), (I) tasks for testing problem-solving skills (T2, T5, T8 and T11), (J) tasks for evaluating short-term (T3, T6, T9 and T12) and (K) long-term memory (T4, T7, T10 and T13) in the puzzle box test. n = 9–11per group. Data are expressed as mean ± S.E.M. Differences were assessed by unpaired two-tailed Student's t-test denoted as follows: $^*p < 0.05$ and $^{**}p < 0.01$ compared with the control group.

Fig. 4. Knockout of PKR in mice ameliorated both laparotomy-induced peripheral and neural inflammation after the surgery. Relative cytokine mRNA expressions were measured in the liver, frontal cortex, and hippocampus of both the C57BL/6J mice and PKR-KO mice at (A) 4 h and (B) 1 day after laparotomy. n = 6 per group. Data are expressed as mean ± S.E.M. Differences were assessed by two-way ANOVA and Bonferroni's post hoc test denoted as follows: $^*p < 0.05$ and $^{**}p < 0.01$, compared with the control group.

Fig. 5. Knockout of PKR in mice ameliorated the activation of microglia in the frontal cortex and hippocampus following laparotomy. Representative confocal images of the immunohistochemical staining of DAPI and Iba1 in the (A) frontal cortex, (C) cornu ammonis (CA) 1, (E) CA3 and (G) dentate gyrus (DG) of the hippocampus sections from PKR-KO mice of the control and laparotomy group on postoperative day 14. The number of Iba1 positive cells, the

relative fluorescence intensity of Iba1 positive cells, the total number of endpoints per Iba1 positive cell, and summed process length per Iba1 positive cell in the (B) frontal cortex, (D) CA1, (F) CA3 and (H) DG of the hippocampus sections were quantified. n = 5 per group. Data are expressed as mean ± S.E.M. Differences were assessed by unpaired two-tailed Student's t-test.

Fig. 6. Genetic deletion of PKR in mice alleviated the laparotomy-induced cognitive impairment. (A) Percentage of the body weight change from baseline of both the C57BL/6J mice and PKR-KO mice during the postoperative period. (B) Total distance travelled and (C) central duration of mice in the open-field test were measured. (D) Discrimination index, which is the ratio of exploration time of one object to two objects, was measured on the novel object recognition test day 1 (with two identical objects: A+A) and (E) day 2 (with a novel object replaced the familiar one: A+B). (F) Total number of arm entries and (G) percentage of alternation were measured in the spontaneous alternation Y-maze test. In the puzzle box test, the latency time for the mice entering the goal zone in different tasks were measured. All the tasks include (H) task for habituation (T1), (I) tasks for testing problem-solving skills (T2, T5, T8 and T11), (J) tasks for evaluating short-term (T3, T6, T9 and T12) and (K) long-term memory (T4, T7, T10 and T13). n = 8–11 per group. Data are expressed as mean ± S.E.M. Differences were assessed by two-way ANOVA and Bonferroni's post hoc test denoted as follows: $^{*}p < 0.05$ and $^{**}p < 0.01$ compared with the control group.

Fig. 7. Inhibition of PKR in cholinergic neurons ameliorated laparotomy-induced cognitive impairment. (A) Percentage of the body weight change from baseline of the ChAT-IRES-Cre-eGFP mice of the control group injected with saline (SAL) and the treatment group injected with the rAAV-DIO-PKR-K296R (AAV) during the postoperative period. (B) Total distance travelled and (C) central duration of mice in the open-field test were measured. (D) Total number of arm entries and (E) percentage of alternation were measured in the spontaneous alternation Y-maze test. In the puzzle box test, the latency time for the mice entering the goal zone in different tasks were measured. All the tasks include (F) task for habituation (T1), (G) tasks for testing problem-solving skills (T2, T5, T8 and T11), (H) tasks for evaluating short-term (T3, T6, T9 and T12) and (I) long-term memory (T4, T7, T10 and T13). n = 6–8 per group. Data are expressed as mean ± S.E.M. Differences were assessed by two-way ANOVA and Bonferroni's post hoc test denoted as follows: $^{*}p < 0.05$, $^{**}p < 0.01$, $^{***}p < 0.001$, $^{****}p < 0.0001$ compared with the control group.

Fig. 8. Inhibition of PKR in cholinergic neurons ameliorated laparotomy-induced changes in glucose metabolism in the frontal cortex. Two-dimensional score plots using the (A) principal component analysis (PCA) and (B) partial least squares discriminant analysis (PLS-DA) were plotted. (C) Heatmap of the metabolites involved in central carbon metabolism in the frontal cortex of the ChAT-IRES-Cre-eGFP mice of the control group received injection of saline (SAL) and the treatment group injected with the rAAV-DIO-PKR-K296R (AAV). Both groups of mice were then randomly divided into the laparotomy and control group. The effects of AAV treatment and laparotomy on glucose metabolism were analyzed using gas chromatography-tandem mass spectrometry (GC-MS/MS). The column represents the samples and the row displays the glucose metabolites. The heatmap scale ranges from −3 to 3. The brightness of each color corresponded to the magnitude of the log2 fold change of the measured metabolites. The concentration of (D) glucose, (E) phosphoenolpyruvate, (F) succinate, and (G) 6-phosphogluconate were quantified in nmol/g. n = 4 per group. Data are expressed as mean ± S.E.M. Differences were assessed by two-way ANOVA and Bonferroni's post hoc test denoted as follows: $^{*}p < 0.05$, $^{**}p < 0.01$, compared with the control group.

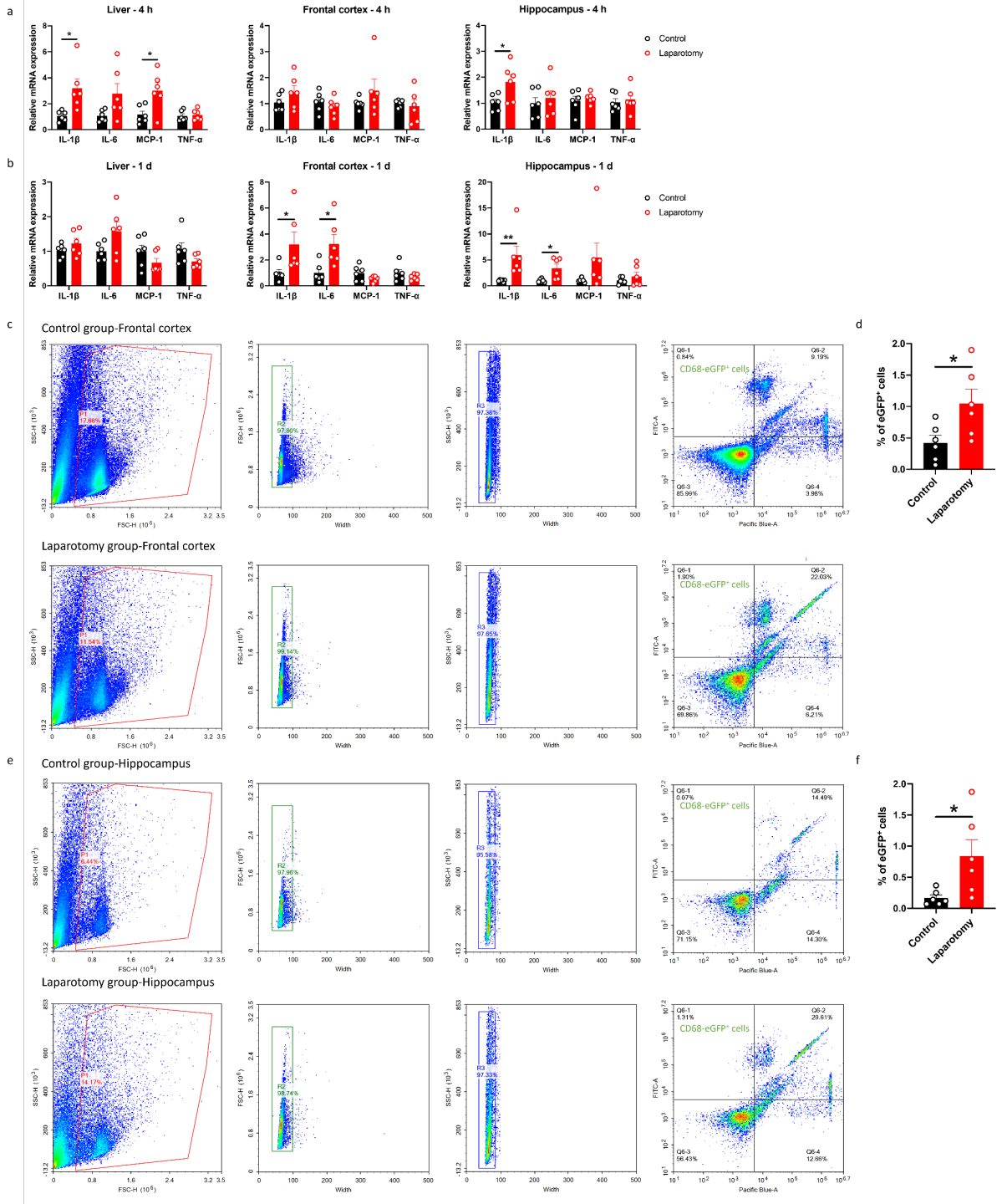
a
Liver - 4 h
Frontal cortex - 4 h
Hippocampus - 4 h
Relative mRNA expression
IL-1β
IL-6
MCP-1
TNF-α
Control
Laparotomy
b
Liver - 1 d
Frontal cortex - 1 d
Hippocampus - 1 d
c
Control group-Frontal cortex
Laparotomy group-Frontal cortex
CD68-eGFP⁺ cells
d
% of eGFP⁺ cells
e
Control group-Hippocampus
Laparotomy group-Hippocampus
f

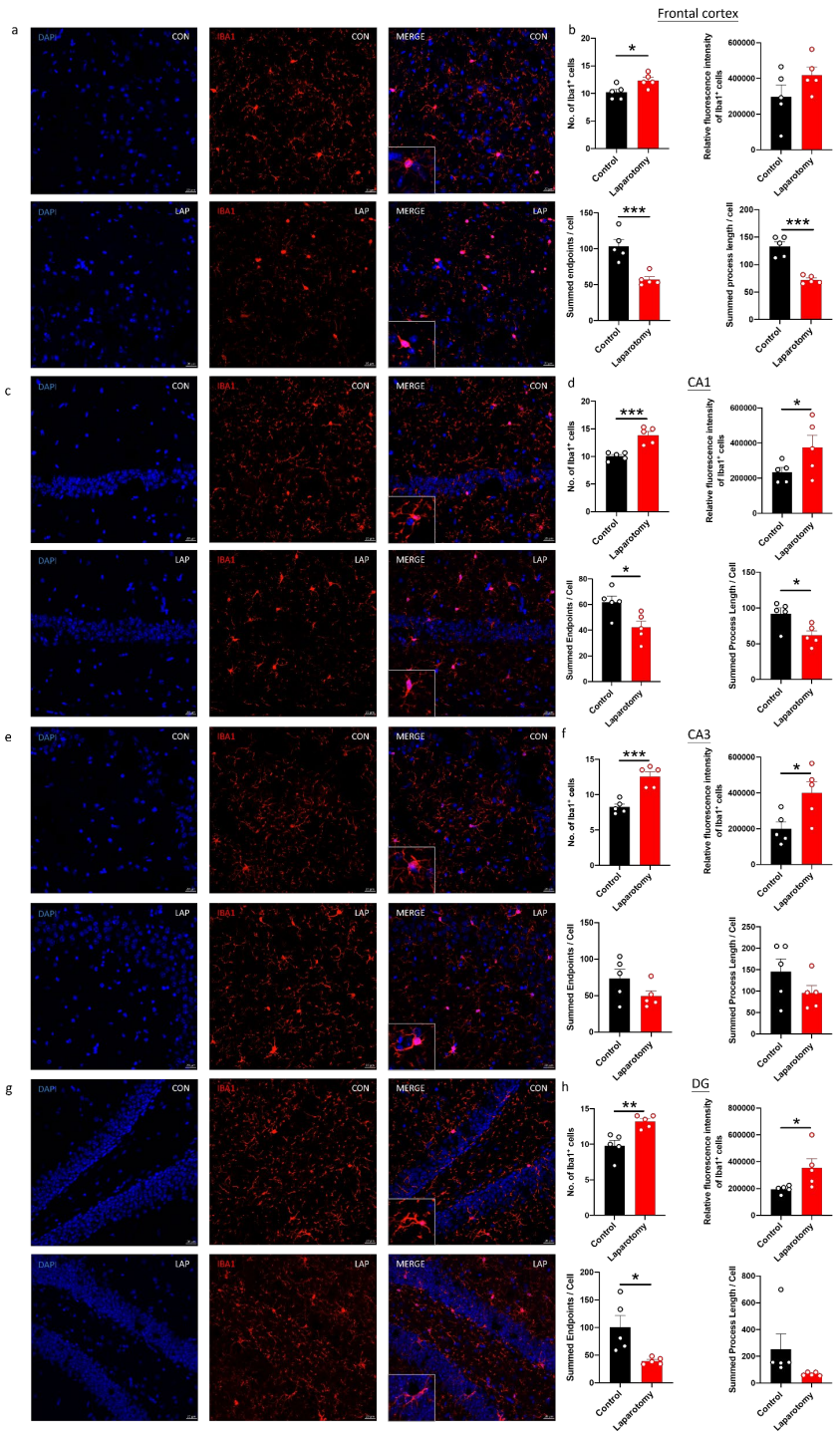
Frontal cortex
a
DAPI
CON
IBA1
MERGE
LAP
b
No. of Iba1⁺ cells
Relative fluorescence intensity of Iba1⁺ cells
Summed endpoints / cell
Summed process length / cell
Control
Laparotomy
c
CA1
d
Summed Endpoints / Cell
Summed Process Length / Cell
e
CA3
f
g
DG
h

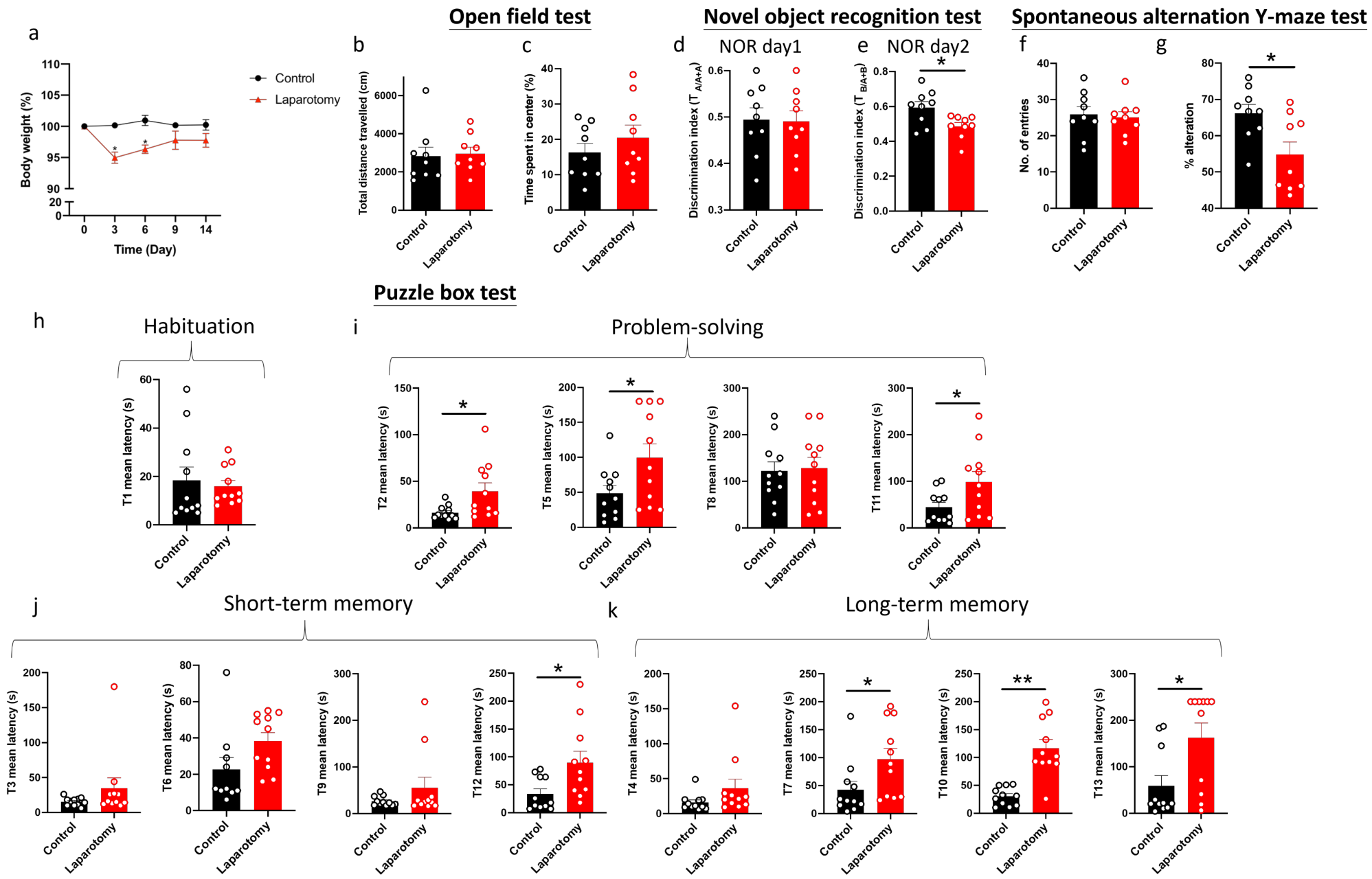
Open field test
Novel object recognition test
Spontaneous alternation Y-maze test
a
Body weight (%)
Time (Day)
Control
Laparotomy
b
Total distance travelled (cm)
c
Time spent in center (%)
d
NOR day1
Discrimination index (T A/A+A)
e
NOR day2
Discrimination index (T B/A+B)
f
No. of entries
g
% alteration
Puzzle box test
h
Habituation
T1 mean latency (s)
i
Problem-solving
T2 mean latency (s)
T5 mean latency (s)
T8 mean latency (s)
T11 mean latency (s)
j
Short-term memory
T3 mean latency (s)
T6 mean latency (s)
T9 mean latency (s)
T12 mean latency (s)
k
Long-term memory
T4 mean latency (s)
T7 mean latency (s)
T10 mean latency (s)
T13 mean latency (s)

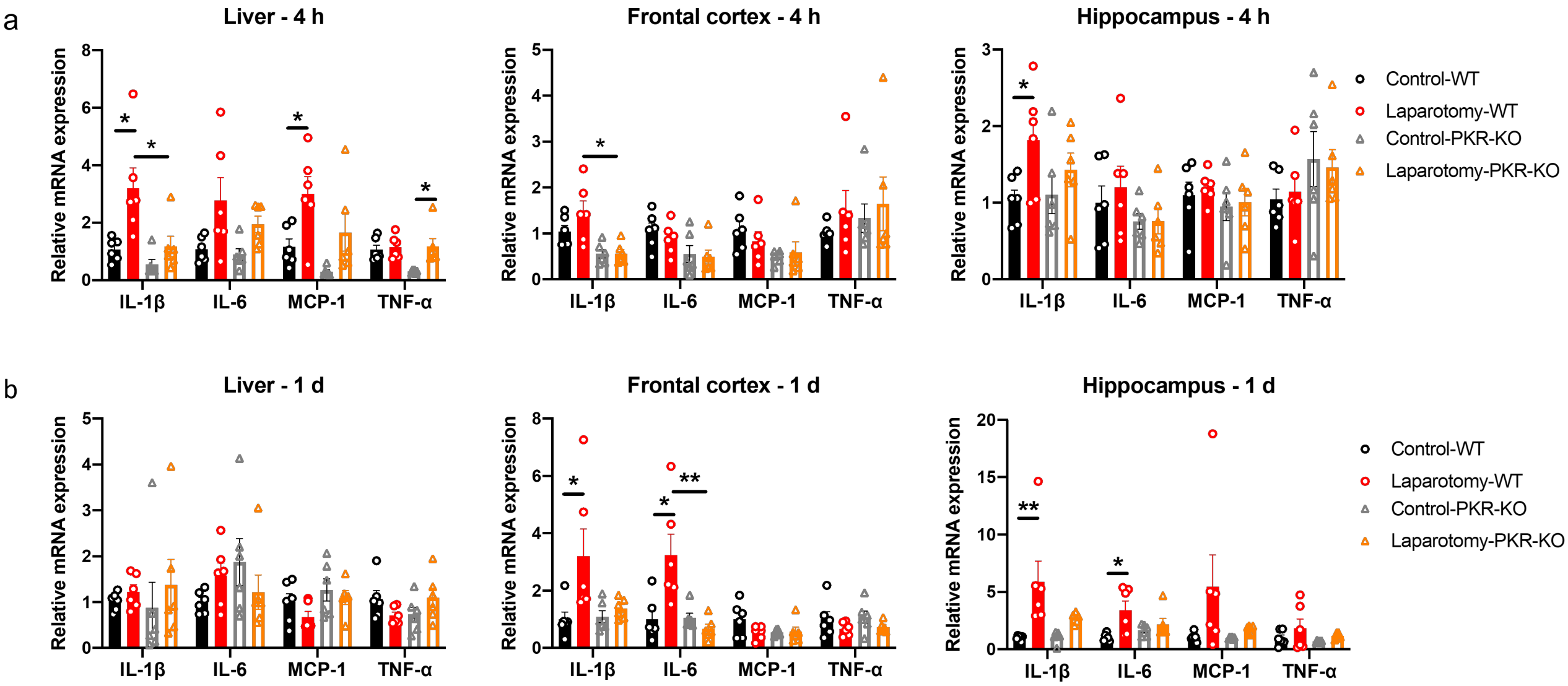
a
Liver - 4 h
Frontal cortex - 4 h
Hippocampus - 4 h
b
Liver - 1 d
Frontal cortex - 1 d
Hippocampus - 1 d
Relative mRNA expression
IL-1β
IL-6
MCP-1
TNF-α
Control-WT
Laparotomy-WT
Control-PKR-KO
Laparotomy-PKR-KO

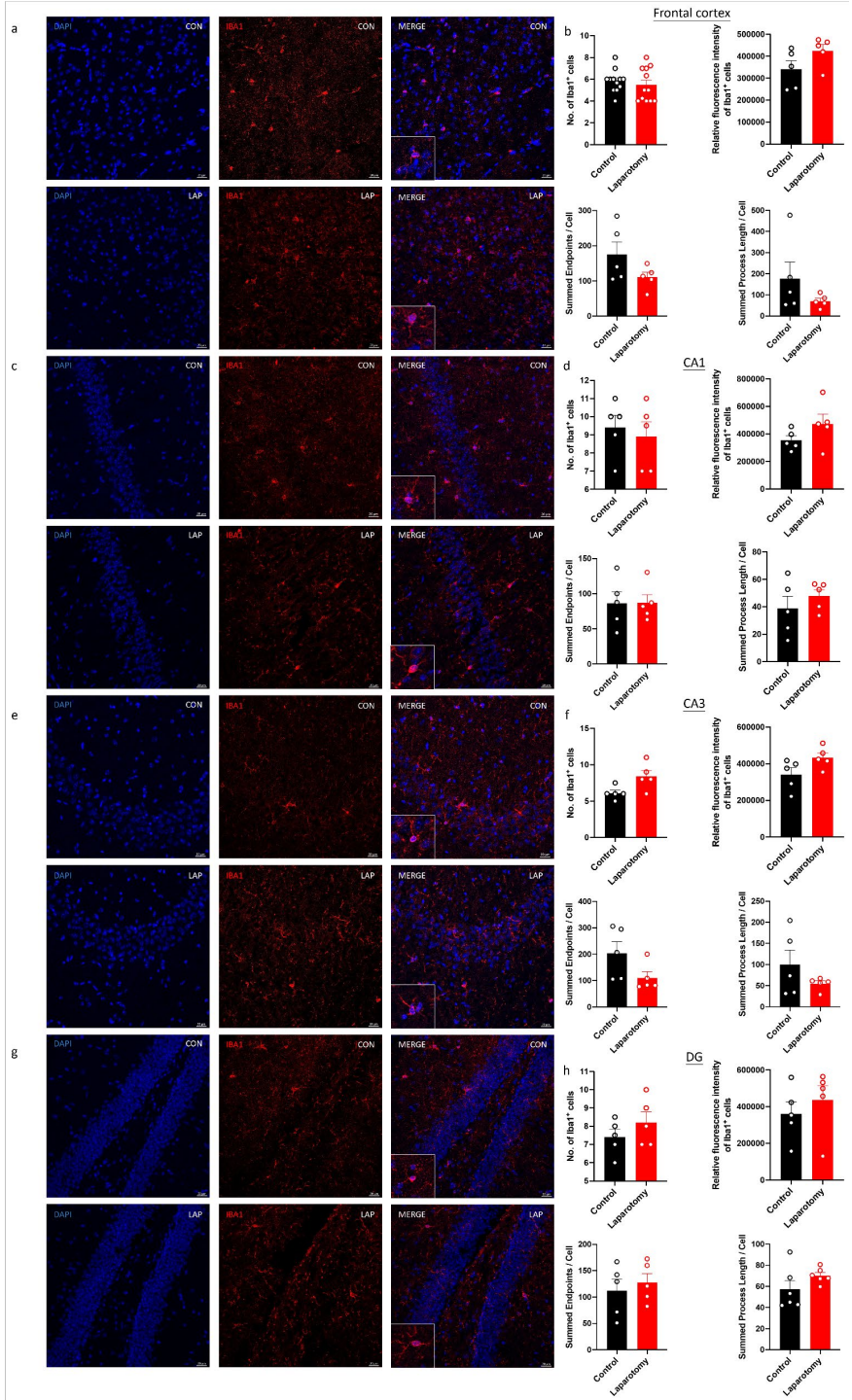
Frontal cortex
a
b
c
d
CA1
e
f
CA3
g
h
DG
DAPI
IBA1
MERGE
CON
LAP
No. of Iba1+ cells
Relative fluorescence intensity of Iba1+ cells
Summed Endpoints / Cell
Summed Process Length / Cell
Control
Laparotomy

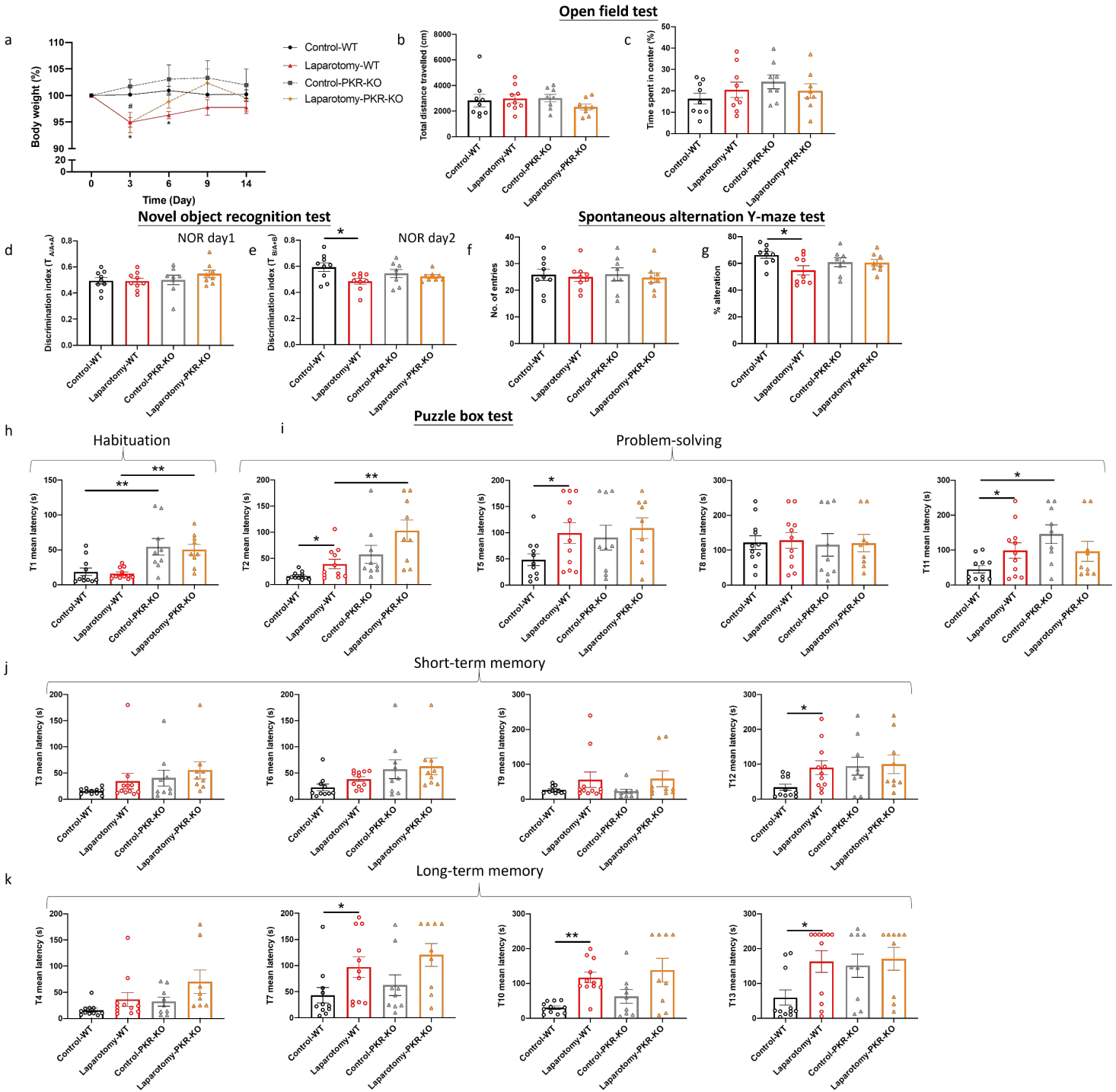
Open field test
a
Body weight (%)
Time (Day)
Control-WT
Laparotomy-WT
Control-PKR-KO
Laparotomy-PKR-KO
b
Total distance travelled (cm)
c
Time spent in center (%)
Novel object recognition test
d
NOR day1
e
NOR day2
Spontaneous alternation Y-maze test
f
No. of entries
g
% alteration
Puzzle box test
h
Habituation
i
Problem-solving
T1 mean latency (s)
T2 mean latency (s)
T5 mean latency (s)
T8 mean latency (s)
T11 mean latency (s)
j
Short-term memory
T3 mean latency (s)
T6 mean latency (s)
T9 mean latency (s)
T12 mean latency (s)
k
Long-term memory
T4 mean latency (s)
T7 mean latency (s)
T10 mean latency (s)
T13 mean latency (s)

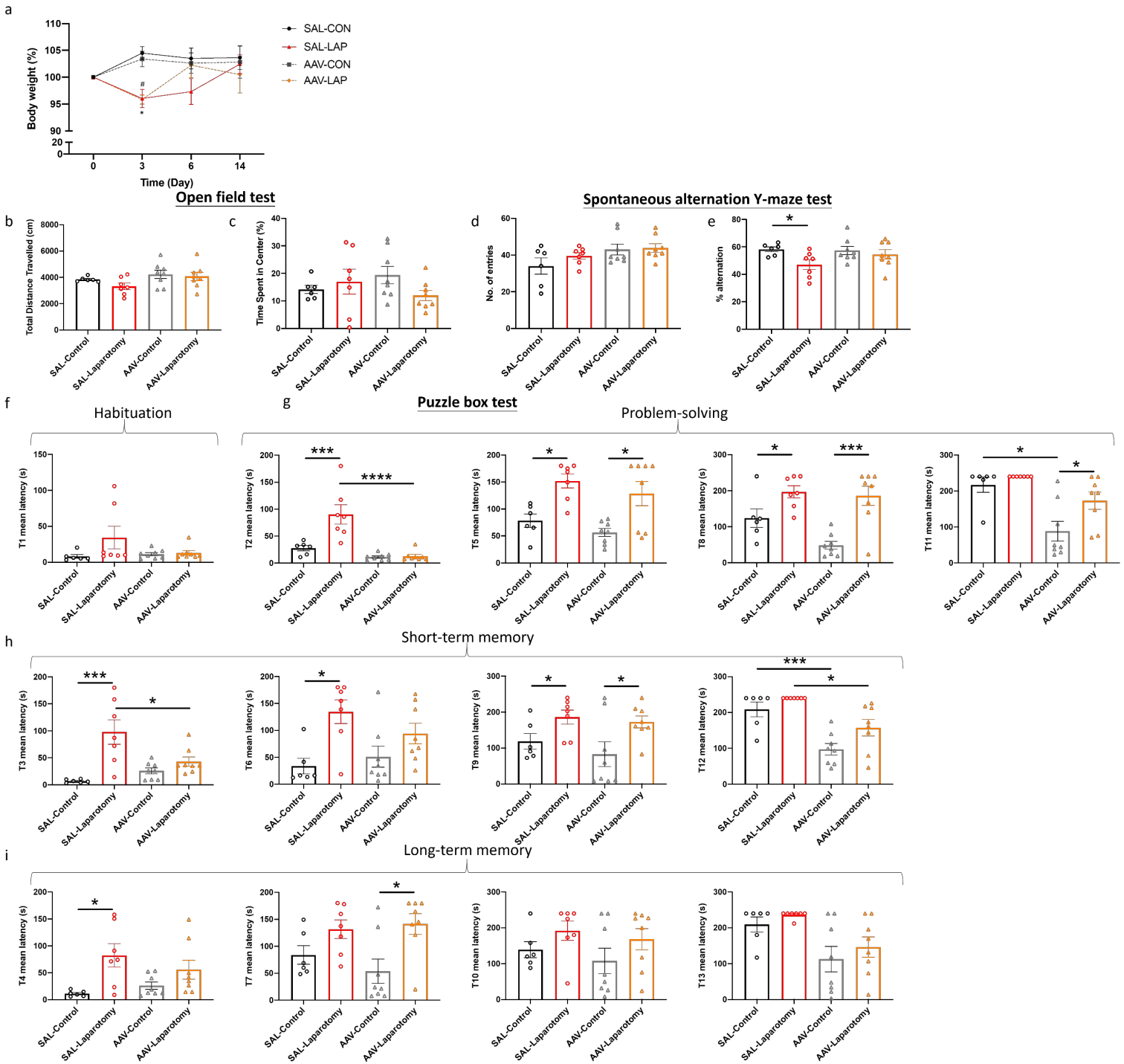
a
Body weight (%)
Time (Day)
SAL-CON
SAL-LAP
AAV-CON
AAV-LAP
Open field test
Spontaneous alternation Y-maze test
b
Total Distance Travelled (cm)
c
Time Spent in Center (%)
d
No. of entries
e
% alternation
SAL-Control
SAL-Laparotomy
AAV-Control
AAV-Laparotomy
f
g
Puzzle box test
Habituation
Problem-solving
T1 mean latency (s)
T2 mean latency (s)
T5 mean latency (s)
T8 mean latency (s)
T11 mean latency (s)
h
Short-term memory
T3 mean latency (s)
T6 mean latency (s)
T9 mean latency (s)
T12 mean latency (s)
i
Long-term memory
T4 mean latency (s)
T7 mean latency (s)
T10 mean latency (s)
T13 mean latency (s)

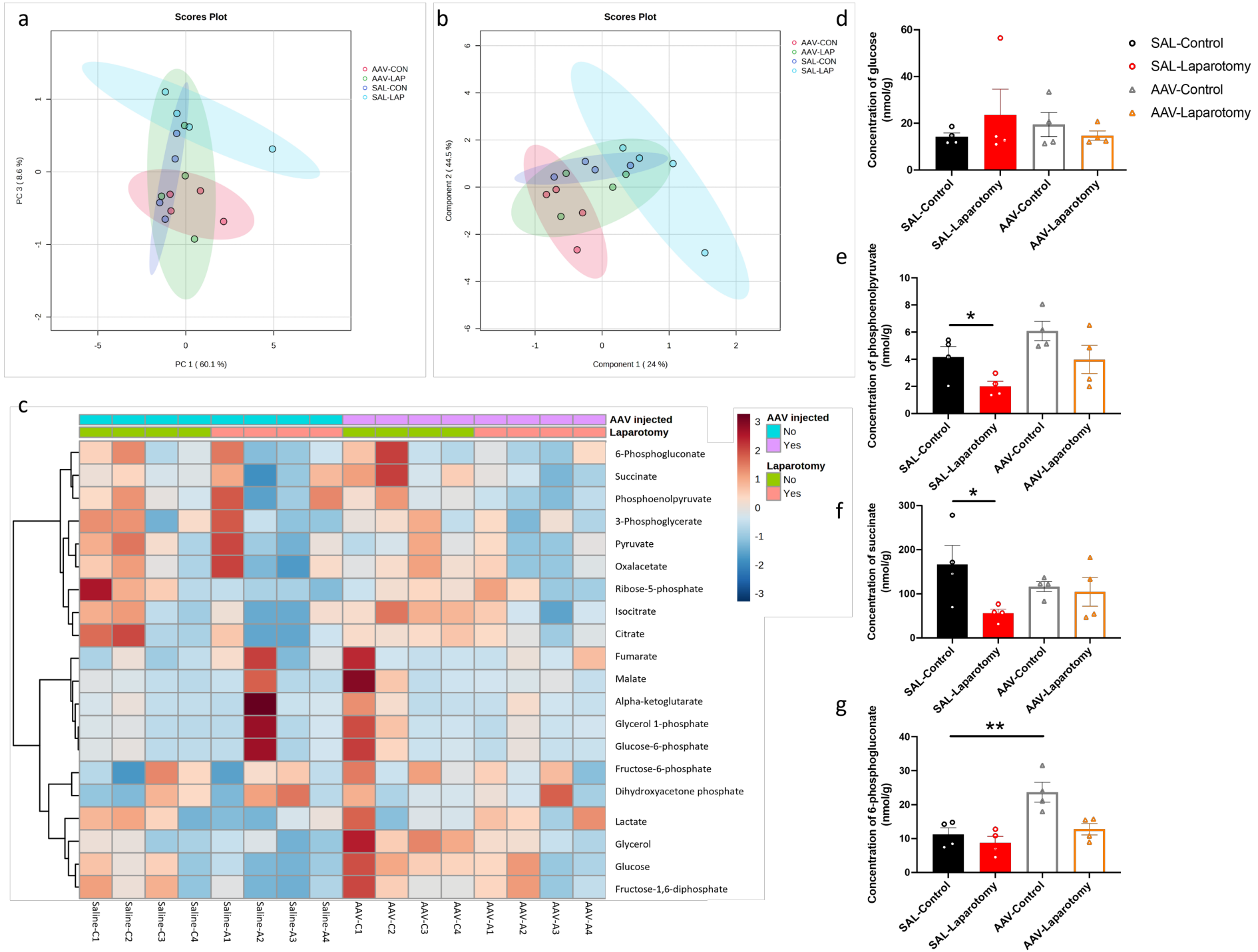
a
Scores Plot
AAV-CON
AAV-LAP
SAL-CON
SAL-LAP
PC 3 (8.6 %)
PC 1 (60.1 %)
b
Scores Plot
Component 2 (44.5 %)
Component 1 (24 %)
c
AAV injected
Laparotomy
6-Phosphogluconate
Succinate
Phosphoenolpyruvate
3-Phosphoglycerate
Pyruvate
Oxalacetate
Ribose-5-phosphate
Isocitrate
Citrate
Fumarate
Malate
Alpha-ketoglutarate
Glycerol 1-phosphate
Glucose-6-phosphate
Fructose-6-phosphate
Dihydroxyacetone phosphate
Lactate
Glycerol
Glucose
Fructose-1,6-diphosphate
Saline-C1
Saline-C2
Saline-C3
Saline-C4
Saline-A1
Saline-A2
Saline-A3
Saline-A4
AAV-C1
AAV-C2
AAV-C3
AAV-C4
AAV-A1
AAV-A2
AAV-A3
AAV-A4
No
Yes
d
Concentration of glucose (nmol/g)
e
Concentration of phosphoenolpyruvate (nmol/g)
f
Concentration of succinate (nmol/g)
g
Concentration of 6-phosphogluconate (nmol/g)
SAL-Control
SAL-Laparotomy
AAV-Control
AAV-Laparotomy